EUROPEAN ORGANIZATION FOR NUCLEAR RESEARCH

CERN-EP-2002-060
17 July 2002

Multi-Photon Production in e^+e^- Collisions at $\sqrt{s} = 181 - 209$ GeV

The OPAL Collaboration

Abstract

The process $e^+e^- \to \gamma\gamma(\gamma)$ is studied using data collected by the OPAL detector at LEP between the years 1997 and 2000. The data set corresponds to an integrated luminosity of 672.3 pb^{-1} at centre-of-mass energies lying between 181 GeV and 209 GeV. Total and differential cross-sections are determined and found to be in good agreement with the predictions of QED. Fits to the observed angular distributions are used to set limits on parameters from several models of physics beyond the Standard Model such as cut-off parameters, contact interactions of the type $e^+e^-\gamma\gamma$, gravity in extra spatial dimensions and excited electrons. In events with three photons in the final state the mass spectrum of photon pairs is investigated. No narrow resonance $X \to \gamma\gamma$ is found and limits are placed on the product of the $X\gamma$ production cross-section and branching ratio.

(To be submitted to the Eur. Phys. J. C)

The OPAL Collaboration

G. Abbiendi[2], C. Ainsley[5], P.F. Åkesson[3], G. Alexander[22], J. Allison[16], P. Amaral[9], G. Anagnostou[1], K.J. Anderson[9], S. Arcelli[2], S. Asai[23], D. Axen[27], G. Azuelos[18,a], I. Bailey[26], E. Barberio[8], R.J. Barlow[16], R.J. Batley[5], P. Bechtle[25], T. Behnke[25], K.W. Bell[20], P.J. Bell[1], G. Bella[22], A. Bellerive[6], G. Benelli[4], S. Bethke[32], O. Biebel[31], I.J. Bloodworth[1], O. Boeriu[10], P. Bock[11], D. Bonacorsi[2], M. Boutemeur[31], S. Braibant[8], L. Brigliadori[2], R.M. Brown[20], K. Buesser[25], H.J. Burckhart[8], S. Campana[4], R.K. Carnegie[6], B. Caron[28], A.A. Carter[13], J.R. Carter[5], C.Y. Chang[17], D.G. Charlton[1,b], A. Csilling[8,g], M. Cuffiani[2], S. Dado[21], G.M. Dallavalle[2], S. Dallison[16], A. De Roeck[8], E.A. De Wolf[8], K. Desch[25], B. Dienes[30], M. Donkers[6], J. Dubbert[31], E. Duchovni[24], G. Duckeck[31], I.P. Duerdoth[16], E. Elfgren[18], E. Etzion[22], F. Fabbri[2], L. Feld[10], P. Ferrari[8], F. Fiedler[31], I. Fleck[10], M. Ford[5], A. Frey[8], A. Fürtjes[8], P. Gagnon[12], J.W. Gary[4], G. Gaycken[25], C. Geich-Gimbel[3], G. Giacomelli[2], P. Giacomelli[2], M. Giunta[4], J. Goldberg[21], E. Gross[24], J. Grunhaus[22], M. Gruwé[8], P.O. Günther[3], A. Gupta[9], C. Hajdu[29], M. Hamann[25], G.G. Hanson[4], K. Harder[25], A. Harel[21], M. Harin-Dirac[4], M. Hauschild[8], J. Hauschildt[25], C.M. Hawkes[1], R. Hawkings[8], R.J. Hemingway[6], C. Hensel[25], G. Herten[10], R.D. Heuer[25], J.C. Hill[5], K. Hoffman[9], R.J. Homer[1], D. Horváth[29,c], R. Howard[27], P. Hüntemeyer[25], P. Igo-Kemenes[11], K. Ishii[23], H. Jeremie[18], P. Jovanovic[1], T.R. Junk[6], N. Kanaya[26], J. Kanzaki[23], G. Karapetian[18], D. Karlen[6], V. Kartvelishvili[16], K. Kawagoe[23], T. Kawamoto[23], R.K. Keeler[26], R.G. Kellogg[17], B.W. Kennedy[20], D.H. Kim[19], K. Klein[11], A. Klier[24], S. Kluth[32], T. Kobayashi[23], M. Kobel[3], S. Komamiya[23], L. Kormos[26], R.V. Kowalewski[26], T. Krämer[25], T. Kress[4], P. Krieger[6,l], J. von Krogh[11], D. Krop[12], K. Kruger[8], M. Kupper[24], G.D. Lafferty[16], H. Landsman[21], D. Lanske[14], J.G. Layter[4], A. Leins[31], D. Lellouch[24], J. Letts[12], L. Levinson[24], J. Lillich[10], S.L. Lloyd[13], F.K. Loebinger[16], J. Lu[27], J. Ludwig[10], A. Macpherson[28,i], W. Mader[3], S. Marcellini[2], T.E. Marchant[16], A.J. Martin[13], J.P. Martin[18], G. Masetti[2], T. Mashimo[23], P. Mättig[m], W.J. McDonald[28], J. McKenna[27], T.J. McMahon[1], R.A. McPherson[26], F. Meijers[8], P. Mendez-Lorenzo[31], W. Menges[25], F.S. Merritt[9], H. Mes[6,a], A. Michelini[2], S. Mihara[23], G. Mikenberg[24], D.J. Miller[15], S. Moed[21], W. Mohr[10], T. Mori[23], A. Mutter[10], K. Nagai[13], I. Nakamura[23], H.A. Neal[33], R. Nisius[8], S.W. O'Neale[1], A. Oh[8], A. Okpara[11], M.J. Oreglia[9], S. Orito[23], C. Pahl[32], G. Pásztor[4,g], J.R. Pater[16], G.N. Patrick[20], J.E. Pilcher[9], J. Pinfold[28], D.E. Plane[8], B. Poli[2], J. Polok[8], O. Pooth[14], M. Przybycień[8,n], A. Quadt[3], K. Rabbertz[8], C. Rembser[8], P. Renkel[24], H. Rick[4], J.M. Roney[26], S. Rosati[3], Y. Rozen[21], K. Runge[10], K. Sachs[6], T. Saeki[23], O. Sahr[31], E.K.G. Sarkisyan[8,j], A.D. Schaile[31], O. Schaile[31], P. Scharff-Hansen[8], J. Schieck[32], T. Schörner-Sadenius[8], M. Schröder[8], M. Schumacher[3], C. Schwick[8], W.G. Scott[20], R. Seuster[14,f], T.G. Shears[8,h], B.C. Shen[4], C.H. Shepherd-Themistocleous[5], P. Sherwood[15], G. Siroli[2], A. Skuja[17], A.M. Smith[8], R. Sobie[26], S. Söldner-Rembold[10,d], S. Spagnolo[20], F. Spano[9], A. Stahl[3], K. Stephens[16], D. Strom[19], R. Ströhmer[31], S. Tarem[21], M. Tasevsky[8], R.J. Taylor[15], R. Teuscher[9], M.A. Thomson[5], E. Torrence[19], D. Toya[23], P. Tran[4], T. Trefzger[31], A. Tricoli[2], I. Trigger[8], Z. Trócsányi[30,e], E. Tsur[22], M.F. Turner-Watson[1], I. Ueda[23], B. Ujvári[30,e], B. Vachon[26], C.F. Vollmer[31], P. Vannerem[10], M. Verzocchi[17], H. Voss[8], J. Vossebeld[8,h], D. Waller[6], C.P. Ward[5], D.R. Ward[5], P.M. Watkins[1], A.T. Watson[1], N.K. Watson[1], P.S. Wells[8], T. Wengler[8], N. Wermes[3], D. Wetterling[11] G.W. Wilson[16,k], J.A. Wilson[1], G. Wolf[24], T.R. Wyatt[16], S. Yamashita[23], D. Zer-Zion[4], L. Zivkovic[24]

[1]School of Physics and Astronomy, University of Birmingham, Birmingham B15 2TT, UK
[2]Dipartimento di Fisica dell' Università di Bologna and INFN, I-40126 Bologna, Italy
[3]Physikalisches Institut, Universität Bonn, D-53115 Bonn, Germany
[4]Department of Physics, University of California, Riverside CA 92521, USA
[5]Cavendish Laboratory, Cambridge CB3 0HE, UK
[6]Ottawa-Carleton Institute for Physics, Department of Physics, Carleton University, Ottawa, Ontario K1S 5B6, Canada
[8]CERN, European Organisation for Nuclear Research, CH-1211 Geneva 23, Switzerland
[9]Enrico Fermi Institute and Department of Physics, University of Chicago, Chicago IL 60637, USA
[10]Fakultät für Physik, Albert-Ludwigs-Universität Freiburg, D-79104 Freiburg, Germany
[11]Physikalisches Institut, Universität Heidelberg, D-69120 Heidelberg, Germany
[12]Indiana University, Department of Physics, Swain Hall West 117, Bloomington IN 47405, USA
[13]Queen Mary and Westfield College, University of London, London E1 4NS, UK
[14]Technische Hochschule Aachen, III Physikalisches Institut, Sommerfeldstrasse 26-28, D-52056 Aachen, Germany
[15]University College London, London WC1E 6BT, UK
[16]Department of Physics, Schuster Laboratory, The University, Manchester M13 9PL, UK
[17]Department of Physics, University of Maryland, College Park, MD 20742, USA
[18]Laboratoire de Physique Nucléaire, Université de Montréal, Montréal, Quebec H3C 3J7, Canada
[19]University of Oregon, Department of Physics, Eugene OR 97403, USA
[20]CLRC Rutherford Appleton Laboratory, Chilton, Didcot, Oxfordshire OX11 0QX, UK
[21]Department of Physics, Technion-Israel Institute of Technology, Haifa 32000, Israel
[22]Department of Physics and Astronomy, Tel Aviv University, Tel Aviv 69978, Israel
[23]International Centre for Elementary Particle Physics and Department of Physics, University of Tokyo, Tokyo 113-0033, and Kobe University, Kobe 657-8501, Japan
[24]Particle Physics Department, Weizmann Institute of Science, Rehovot 76100, Israel
[25]Universität Hamburg/DESY, Institut für Experimentalphysik, Notkestrasse 85, D-22607 Hamburg, Germany
[26]University of Victoria, Department of Physics, P O Box 3055, Victoria BC V8W 3P6, Canada
[27]University of British Columbia, Department of Physics, Vancouver BC V6T 1Z1, Canada
[28]University of Alberta, Department of Physics, Edmonton AB T6G 2J1, Canada
[29]Research Institute for Particle and Nuclear Physics, H-1525 Budapest, P O Box 49, Hungary
[30]Institute of Nuclear Research, H-4001 Debrecen, P O Box 51, Hungary
[31]Ludwig-Maximilians-Universität München, Sektion Physik, Am Coulombwall 1, D-85748 Garching, Germany
[32]Max-Planck-Institute für Physik, Föhringer Ring 6, D-80805 München, Germany
[33]Yale University, Department of Physics, New Haven, CT 06520, USA

[a] and at TRIUMF, Vancouver, Canada V6T 2A3
[b] and Royal Society University Research Fellow
[c] and Institute of Nuclear Research, Debrecen, Hungary
[d] and Heisenberg Fellow
[e] and Department of Experimental Physics, Lajos Kossuth University, Debrecen, Hungary
[f] and MPI München

[g] and Research Institute for Particle and Nuclear Physics, Budapest, Hungary
[h] now at University of Liverpool, Dept of Physics, Liverpool L69 3BX, UK
[i] and CERN, EP Div, 1211 Geneva 23
[j] and Universitaire Instelling Antwerpen, Physics Department, B-2610 Antwerpen, Belgium
[k] now at University of Kansas, Dept of Physics and Astronomy, Lawrence, KS 66045, USA
[l] now at University of Toronto, Dept of Physics, Toronto, Canada
[m] current address Bergische Universität, Wuppertal, Germany
[n] and University of Mining and Metallurgy, Cracow, Poland

1 Introduction

This paper presents a study of the process $e^+e^- \to \gamma\gamma(\gamma)$, where the brackets indicate a possible third particle that might escape along the beam direction. Data with a total integrated luminosity of 672.3 pb^{-1} collected in the years 1997 to 2000 with the OPAL detector at LEP at centre-of-mass energies between 181 GeV and 209 GeV are used. This process is one of the few reactions which are dominated by QED even at these energies. The high statistics sample considered in this paper allows precision tests of QED and searches for new particles such as excited electrons and photonically decaying resonances.

This process has been studied previously at LEP at lower energies [1–3] and by other experiments [4–11]. The increased data sample since our last publication leads to a much better understanding of the detector and the systematic errors. In addition the selection efficiency has been increased. Therefore this paper includes a re-analysis of previously published data at 183 GeV and 189 GeV [2, 3] and supersedes those results. Total and differential cross-sections are determined and compared with the predictions of QED.

There are several models which predict deviations from the QED cross-section introducing cut-off parameters [12], $e^+e^-\gamma\gamma$ contact interactions [13], the exchange of excited electrons [14, 15] or the exchange of Kaluza-Klein gravitons in models with extra dimensions [16]. The measured differential cross-sections are used to place constraints on the parameters of these models.

The search for a resonance X which is produced along with a photon and decays via $X \to \gamma\gamma$ is especially interesting in the light of models with fermiophobic Higgs bosons [17] or hypercharge axions [18]. Because of the higher kinematic reach the three-photon final state is complementary to ZX production. Events with three observed photons are used to search for such a resonance. Similar searches were performed previously at the Z peak [19] and at lower LEP2 energies [1–3, 20].

In the next section a short description of the relevant detector components is given. This is followed by an overview of the data and Monte Carlo samples used in the analysis. Section 4 contains an introduction to the theoretical models. The event selection is described in Section 5, the systematic errors are summarised in Section 6 and the results are given in Section 7.

2 The OPAL detector

A detailed description of the OPAL detector can be found elsewhere [21, 22] so only those components most relevant to this analysis are discussed here.

The most important subdetector for this analysis is the electromagnetic calorimeter (ECAL). The barrel region[1] ($|\cos\theta| < 0.82$) consists of 9440 lead-glass blocks in a quasi-pointing geometry each with a cross-section of about 10×10 cm at an inner radius of 2.45 m. The two

[1] OPAL uses a right-handed coordinate system in which the z axis is along the electron beam direction, x points to the centre of LEP such that the y axis points approximately upwards. The polar angle, θ, is measured with respect to the z axis and the azimuthal angle, ϕ, with respect to the x axis.

endcaps ($0.81 < |\cos\theta| < 0.98$) consist of 1132 blocks each, aligned parallel to the beam axis. The inner faces are placed at a z position of about ± 2.3 m. For beam-energy photons, the spatial resolution is about 11 mm, corresponding to an uncertainty of 0.2° in θ, and the energy resolution is about 2% in the barrel and 3% – 5% in the endcaps, depending on the polar angle.

The ECAL surrounds the tracking chambers. The large volume jet chamber (CJ) has an outer diameter of 3.7 m and is about 4 m long. It is segmented into 24 sectors each containing 159 axial sense wires. The vertex chamber (CV) has an outer diameter of 47 cm and is 1 m long. It is segmented into 36 sectors each containing 12 axial wires in the inner region and an outer region of 6 stereo wires. CV and CJ are inside a common pressure vessel and separated by a foil and a carbon fibre tube. A silicon micro-vertex detector (SI) is located between CV and the beam pipe, at a radius of about 7 cm. This subdetector consists of two layers of double sided (z and ϕ sensitive) ladders. The inner (outer) layer covers $|\cos\theta| < 0.93$ (0.89) and has a ϕ acceptance of 97.8% (99.6%).

Outside the ECAL the instrumented return yoke serves as a hadronic calorimeter. The outermost subdetector is the muon system which consists of up to 4 layers of drift chambers. The luminosity is measured using small-angle Bhabha events collected in the silicon-tungsten luminometer [23].

3 Data sample and Monte Carlo simulation

Table 1 lists the data samples analysed in this paper. They are from the last four years of LEP running with a total of 5235 selected events taken at centre-of-mass energies between 181 GeV and 209 GeV. As an example, the last $e^+e^- \to \gamma\gamma(\gamma)$ event, which was recorded three minutes before the final shut down of LEP, is shown in Figure 1. Two photons, back-to-back in ϕ, are observed in the detector. One photon has converted between CV and CJ. From the acollinearity a third photon is deduced to have escaped along the beam direction.

Various Monte Carlo samples are used to study the selection efficiency and expected back-

year	$\sqrt{s}_{\rm nom}$	$\sqrt{s}_{\rm range}$ [GeV]	$\sqrt{s}$ [GeV]	luminosity [pb^{-1}]	events
1997	183	180.8−184.0	182.68	55.57±0.15±0.19	538
1998	189	188.6−189.0	188.63	181.07±0.16±0.36	1531
1999	192	191.4−192.0	191.59	29.03±0.06±0.07	258
1999	196	195.2−196.0	195.53	75.92±0.10±0.16	616
99/00	200	199.4−200.2	199.52	78.20±0.11±0.17	554
99/00	202	201.4−202.5	201.63	36.78±0.07±0.08	281
2000	205	202.5−205.5	204.88	79.22±0.11±0.17	566
2000	207	205.5−209.0	206.56	136.49±0.14±0.30	891

Table 1: Data used in this paper. The year of data taking, the nominal centre-of-mass energy, the energy range, the luminosity-weighted mean centre-of-mass energy, the integrated luminosity with its statistical and systematic error and the number of selected events are shown.

ground contributions. The signal $e^+e^- \to \gamma\gamma(\gamma)$ events are generated using the RADCOR [24] generator which relies on a full $\mathcal{O}(\alpha^3)$ calculation taking the electron mass into account. Events with four observed photons can be simulated using FGAM [25] which contains a lowest-order relativistic calculation of four-photon production. Bhabha events are simulated using BHWIDE [26] ($e^+e^-(\gamma)$) and TEEGG [27] ($e\gamma(e)$). For $e^+e^- \to \nu\bar{\nu}\gamma(\gamma)$ events KORALZ [28] and NUNUGPV [29] are used. Tau pairs are simulated using KORALZ [28], and PYTHIA [30, 31] is used for hadronic events. All samples are processed through the OPAL detector simulation program [32] and reconstructed in the same way as the data.

4 Cross-section for the process $e^+e^- \to \gamma\gamma(\gamma)$

4.1 QED Born cross-section

Up to the highest LEP energies the process $e^+e^- \to \gamma\gamma(\gamma)$ can be described by QED. The lowest order cross-section in the relativistic limit is given by:

$$\left(\frac{d\sigma}{d\cos\theta}\right)_{\text{Born}} = \frac{2\pi\ \alpha^2}{s}\ \frac{1+\cos^2\theta}{1-\cos^2\theta}\ , \tag{1}$$

where $\sqrt{s}$ is the centre-of-mass energy and α is the fine-structure constant at zero momentum transfer. The non-relativistic cross-section formula is given in [33]. Since the final-state particles are identical, the polar angle θ is defined such that $\cos\theta > 0$. At Born level the definition of θ is unambiguous since the two photons are back-to-back. The definition at higher orders used in this paper is given in Section 4.2.

Weak interactions contribute only via loop diagrams. At the W-pair threshold weak corrections of up to 1.2% are expected for $\cos\theta = 0$ [34, 35]. At the energies considered in this analysis the corrections are smaller, e.g. for a centre-of-mass energy of 200 GeV they are less than 0.2% for all angles, and will be neglected.

4.2 Radiative corrections

In the presence of higher order effects the measured angular distribution depends not only on one angle θ but on the angles of all produced photons. To enable a comparison of the measurement with Equation 1 an event angle must be defined to substitute θ. Various definitions of the event angle are possible, each leading to a different measured angular distribution. The ratio of this physical distribution to the distribution from the Born-level prediction is called a radiative correction $\mathcal{R}$. The event angle θ^* used in this analysis is defined by:

$$\cos\theta^* = \left|\sin\frac{\theta_1-\theta_2}{2}\right| \Big/ \left(\sin\frac{\theta_1+\theta_2}{2}\right)\ , \tag{2}$$

where θ_1 and θ_2 are the angles of the two highest-energy photons. At Born level $\cos\theta = \cos\theta^*$. The angle θ^* is equivalent to the angle in the centre-of-mass system of the two highest-energy

photons unless a third photon is produced away from the beam direction. With this definition, deviations of $\mathcal{R}$ from unity are relatively small and uniform as determined from an $\mathcal{O}(\alpha^3)$ Monte Carlo [24] without detector simulation. Using high statistics samples of 10^9 events, generated at centre-of-mass energies of 189 GeV, 200 GeV and 206 GeV, the correction $\mathcal{R}$ is found to depend only weakly on the centre-of-mass energy. Therefore the $\sqrt{s}$ dependence is neglected. The average correction for $\cos\theta^* < 0.93$ is $\mathcal{R} = 1.0448$; the angular dependence can be found in Table 6. For QED processes the effects due to the next order can be assumed to be about 10% of the corrections at this order. Since no fourth order Monte Carlo generator is available and weak contributions are neglected, a systematic error of 0.01 is assumed for the radiative correction. The ratio $\mathcal{R}$ is used to correct the measured cross-sections presented in this paper to the Born level.

4.3 Alternative models

Various models predict deviations from the QED expectation[2]. The simplest ansatz is a short-range exponential deviation from the Coulomb field parameterised by cut-off parameters $\Lambda_\pm$ [12]. This leads to a differential cross-section of the form

$$\left(\frac{d\sigma}{d\cos\theta}\right)_{\Lambda_\pm} = \left(\frac{d\sigma}{d\cos\theta}\right)_{\text{Born}} \pm \frac{\alpha^2\pi s}{\Lambda_\pm^4}(1+\cos^2\theta)\ . \tag{3}$$

New effects can also be introduced in effective Lagrangian theory [13]. Here dimension-6 terms lead to anomalous eeγ couplings. The resulting deviations in the differential cross-section are similar in form to those given in Equation 3, but with a slightly different definition of the parameter: $\Lambda_6^4 = \frac{2}{\alpha}\Lambda_+^4$. Dimension 7 and 8 Lagrangians introduce ee$\gamma\gamma$ contact interactions and result in an angle-independent term added to the Born cross-section:

$$\left(\frac{d\sigma}{d\cos\theta}\right)_{\Lambda'} = \left(\frac{d\sigma}{d\cos\theta}\right)_{\text{Born}} + \frac{s^2}{16}\frac{1}{\Lambda'^6}\ . \tag{4}$$

The associated parameters are given by $\Lambda_7 = \Lambda'$ and $\Lambda_8^4 = m_{\mathrm{e}}\Lambda'^3$ for dimension 7 and dimension 8 couplings, respectively. The subscript refers to the dimension of the Lagrangian.

Instead of an ordinary electron, an excited electron e^* with mass M_{e^*} could be exchanged in the t-channel [14, 15]. In the most general case $\mathrm{e}^*\mathrm{e}\gamma$ couplings would lead to a large anomalous magnetic moment of the electron [36, 37]. This effect can be avoided by a chiral magnetic coupling of the form

$$\mathcal{L}_{\mathrm{e}^*\mathrm{e}\gamma} = \frac{1}{2\Lambda}\bar{e^*}\sigma^{\mu\nu}\left[gf\frac{\tau}{2}W_{\mu\nu} + g'f'\frac{Y}{2}B_{\mu\nu}\right]e_L + \text{h.c.}\ , \tag{5}$$

where τ are the Pauli matrices and Y is the hypercharge. The parameters of the model are the compositeness scale Λ and the weight factors f and f' associated to the gauge fields W and B with Standard Model couplings g and g'. For the process $\mathrm{e}^+\mathrm{e}^- \to \gamma\gamma(\gamma)$, the following cross-section results [38]:

[2] All cross-sections given here are to lowest order.

$$\left(\frac{d\sigma}{d\cos\theta}\right)_{\mathrm{e}^*} = \left(\frac{d\sigma}{d\cos\theta}\right)_{\mathrm{Born}} + \frac{\alpha^2\pi}{2}\frac{f_\gamma^4}{\Lambda^4}M_{\mathrm{e}^*}^2\left[\frac{p^4}{(p^2-M_{\mathrm{e}^*}^2)^2}+\frac{q^4}{(q^2-M_{\mathrm{e}^*}^2)^2}+\frac{\frac{1}{2}s^2\sin^2\theta}{(p^2-M_{\mathrm{e}^*}^2)(q^2-M_{\mathrm{e}^*}^2)}\right], \tag{6}$$

with $f_\gamma = -\frac{1}{2}(f+f')$, $p^2 = -\frac{s}{2}(1-\cos\theta)$ and $q^2 = -\frac{s}{2}(1+\cos\theta)$. Effects vanish in the case of $f = -f'$.

Theories of quantum gravity in extra spatial dimensions could solve the hierarchy problem because gravitons would be allowed to travel in more than 3+1 space-time dimensions [39]. While in these models the Planck mass M_D in $D = n+4$ dimensions is chosen to be of electroweak scale the usual Planck mass M_{Pl} in four dimensions would be

$$M_{\mathrm{Pl}}^2 = R^n M_D^{n+2}\ , \tag{7}$$

where R is the compactification radius of the additional dimensions. Since gravitons couple to the energy-momentum tensor, their interaction with photons is as weak as with fermions. However, the huge number of Kaluza-Klein excitation modes in the extra dimensions may give rise to observable effects. These effects depend on the scale $M_s(\sim M_D)$ which may be as low as $\mathcal{O}$(TeV). Model dependencies are absorbed in the parameter λ which is expected to be of $\mathcal{O}(1)$. For this analysis it is assumed that $\lambda = \pm 1$. The expected differential cross-section is given by [16]:

$$\left(\frac{d\sigma}{d\cos\theta}\right)_{M_s} = \left(\frac{d\sigma}{d\cos\theta}\right)_{\mathrm{Born}} - \alpha s\ \frac{\lambda}{M_s^4}\ (1+\cos^2\theta) + \frac{s^3}{8\pi}\ \frac{\lambda^2}{M_s^8}\ (1-\cos^4\theta)\ . \tag{8}$$

5 Event selection

Multi-photon events have a very clear experimental signature. They have large energy deposits in the electromagnetic calorimeter and small missing transverse momentum. They share these properties with Bhabha events ($\mathrm{e^+e^-} \to \mathrm{e^+e^-}(\gamma)$), which represent the most important background. The first stage of the event selection is a preselection which requires events to have photon candidates and a low multiplicity of tracks and clusters. Cuts are then applied to reject cosmic-ray background. This is followed by a kinematic selection based on the signature of the energy deposit in the ECAL. The last step is a neutral event selection designed to reject Bhabha events using information from the tracking chambers. After application of all selection criteria the total background is reduced to an almost negligible level.

5.1 Preselection

A photon candidate is defined here as an ECAL cluster with an energy of at least 1 GeV and a polar angle satisfying $|\cos\theta| < 0.97$. The cluster must consist of at least two ECAL blocks to ensure a good determination of the photon angle.

The preselection is very loose, requiring at least two photon candidates and a total ECAL energy in the event of at least $0.1\sqrt{s}$. High multiplicity events are rejected by restricting the sum of the number of tracks and ECAL clusters to ≤ 17.

The two highest-energy photons must be within $|\cos\theta| < 0.93$. This avoids a region where the detector material is not sufficiently well modelled to ensure a good description of the conversion probability and the angular reconstruction. The search for a resonance X is based on three-photon events and the invariant mass of X is calculated from the photon angles. Only events in which all three photons are in the region $|\cos\theta| < 0.93$ are used for this search.

5.2 Cosmic-ray background rejection

A cosmic-ray particle can create signals in the outer detectors without producing a reconstructed track in the central tracking chambers. These particles do not necessarily pass close to the beam axis. Since the hadronic and electromagnetic calorimeters have different radii, the resulting hits in the two detectors occur separated in azimuth. Background of this type is suppressed using information from the muon chambers and the hadronic calorimeter. Events are rejected if there are three or more track segments reconstructed in the muon chambers. Events are also rejected if the highest-energy hadronic cluster is separated from each photon candidate by at least 10° in ϕ and has an energy of more than 20% of the summed energy of the photon candidates. In the case of one or two muon track segments the latter cut is tightened to 10%. Additionally, events are rejected if there is a track with a momentum of more than 10 GeV separated from each of the photon candidates by more than 10° in ϕ.

5.3 Kinematic event selection

Events are selected if they have large total energy and small missing transverse momentum. To improve the resolution on these quantities the information on the angle of the cluster is used instead of the energy information where possible. To facilitate this, the events are divided into four classes (*I*, *II*, *III* and *IV*) according to the number of photon candidates N_γ, the acollinearity $\xi_{\text{acol}} = 180° - \alpha_{12}$ and the aplanarity $\xi_{\text{aplan}} = 360° - (\alpha_{12} + \alpha_{13} + \alpha_{23})$, where α_{ij}

<table>
<tr><td>$\xi_{\text{acol}} < 10°$</td><td colspan="3">$\xi_{\text{acol}} > 10°$</td></tr>
<tr><td rowspan="4">I</td><td>II</td><td colspan="2">$N_\gamma = 2$</td></tr>
<tr><td>III</td><td>$\xi_{\text{aplan}} < 0.1°$</td><td>$N_\gamma$</td></tr>
<tr><td rowspan="2">IV</td><td>$\xi_{\text{aplan}} > 0.1°$</td><td>$= 3$</td></tr>
<tr><td colspan="2">$N_\gamma \geq 4$</td></tr>
</table>

Table 2: Definition of classes *I*, *II*, *III* and *IV*. All collinear events are contained in class *I*. Other events are distributed according to the number of photon candidates N_γ and the aplanarity ξ_{aplan}.

is the angle between photon candidates i and j. Here and in the following sections the photon candidates are ordered by energy. The class definitions are shown in Table 2.

Cuts are applied on the energy sum as well as on the missing transverse and longitudinal momenta. The energy sum E_S is defined as the sum of the photon candidate energies E_i plus the missing longitudinal momentum which could originate from a photon escaping along the beam direction. The detailed definitions of these quantities depend on the event class. However the cuts summarised in Table 3 namely that the energy sum must be at least 60% of the centre-of-mass energy and the missing transverse momentum must be less than 10% of the centre-of-mass energy are equivalent. Since the event angle is defined using the two highest-energy photons, events are rejected if one of these escapes detection, that is if the missing longitudinal momentum is larger than the energy of the second highest-energy photon candidate. This cut on the missing longitudinal momentum is not designed to reject background but ensures a good signal definition since it prevents ambiguous events from entering the signal sample. Distributions of the relevant quantities are shown in Figure 2.

Class *I* contains collinear events which make up about 90% of the total sample. For these events it is assumed that missing transverse and longitudinal momenta are negligible, so no cuts on these quantities are applied. The energy sum is simply taken to be $E_S^I = E_1 + E_2$. A class *II* event has exactly two observed photon candidates; since the event is acollinear a third photon is assumed along the beam direction. Quantities $\mathcal{B}$ and $E_{\rm lost}$, equivalent to the missing transverse and longitudinal momenta, are calculated assuming three-body kinematics and are given by:

$$\mathcal{B} = \sqrt{s}/2 \cdot (\sin\theta_1 + \sin\theta_2)\,|\cos\left[(\phi_1 - \phi_2)/2\right]| \ , \tag{9}$$

$$E_{\rm lost} = \sqrt{s}/\left[1 + (\sin\theta_1 + \sin\theta_2)/|\sin\left(\theta_1 + \theta_2\right)|\right] \ . \tag{10}$$

Consequently $E_S^{II} = E_1 + E_2 + E_{\rm lost}$. For classes *III* and *IV* the missing transverse and longitudinal momenta, $p_{\rm t}$ and $p_{\rm l}$, are calculated in the usual way from cluster energies and angles and $E_S^{III} = \sum_i E_i + p_{\rm l}$.

event class	*I*	*II*	*III*, *IV*	cut
energy sum	E_S^I	E_S^{II}	E_S^{III}	$> 0.6\sqrt{s}$
transverse momentum	–	$\mathcal{B}$	$p_{\rm t}$	$< 0.1\sqrt{s}$
longitudinal momentum	–	$E_{\rm lost}$	$p_{\rm l}$	$< E_1, E_2$

Table 3: Cuts for the kinematic event selection. The cut variables depend on the class, see text. For class *I* events no cuts on the missing longitudinal and transverse momenta are applied.

5.4 Neutral event selection

Events without charged particles produced at the primary interaction point are referred to here as neutral events. They are selected using information about the hits in the two main tracking chambers CJ and CV. A photon candidate is said to have hits in one of these chambers if more

than about 50% of the innermost wires in the sector pointing to the photon have hits. For CV the 12 axial layers are taken into account and for CJ the inner 16 layers.

Events are rejected in either of the following two cases:
1) double veto: at least two photon candidates have hits in CV.
2) single veto: any photon candidate has hits in both CV and CJ, unless it is identified as a conversion. To be identified as a conversion, information from the SI detector is necessary and therefore this condition is restricted to $|\cos\theta| < 0.89$. A conversion must have exactly two tracks reconstructed in a three dimensional cone of half angle 20° around the cluster, with at least one of the tracks assigned to the cluster. Additionally, the two SI ladders in the ϕ direction of the cluster must have no more than two hits. Dead ladders are counted as hits to ensure a good background rejection. The two sides of each ladder are counted separately, leading to a maximum number of four hits. Events are rejected if any photon with $|\cos\theta| \geq 0.89$ has hits in CV and CJ.

5.5 Summary

The numbers of events selected and expected after each step of the selection are given in Table 4. The preselection is very loose and there are more events observed after the preselection than expected from the listed Monte Carlo samples. This excess is mainly due to cosmic-ray events and four-fermion events with two observed electrons. The difference between the number of observed and expected events becomes much smaller after the rejection of cosmic-ray background. After the kinematic cuts the sample consists mainly of Bhabha events and the signal efficiency remains at almost 100%. The cut on the longitudinal momentum rejects events with a high-energy particle along the beam direction. For Bhabhas these are mainly events in which one electron escapes and the second electron and a photon are observed in the detector (eγ(e) topology). Most of the remaining Bhabha events have both electrons in the

cut	data	ΣMC	$\gamma\gamma(\gamma)$	$e^+e^-(\gamma)$	eγ(e)	$\nu\bar{\nu}\gamma(\gamma)$	$q\bar{q}(\gamma)$	$\tau^+\tau^-(\gamma)$
preselection	192558	123751	5826	107791	7280	105	398	2352
cosmic bkg.	133099	122898	5823	107697	7194	104	244	1835
kinematic cuts	120515	119674	5809	107048	6310	6.6	130	370
longitudinal mom.	108832	110082	5520	103833	539	0.55	68	122
double veto	6367	6152	5505	68	515	0.55	52	12
single veto	5235	5261	5258	0.38	1.55	0.55	1.10	0.05
		±12	±12	±0.19	±0.43	±0.09	±0.24	±0.03

Table 4: The number of events observed in data after the cuts, the signal expectation and the most important background sources indicated by their final state are given. The row labelled kinematic cuts contains only the cuts on the energy sum and the missing transverse momentum; the cut on the missing longitudinal momentum is listed separately. The neutral event selection is split up into the double veto and the single veto. For the numbers of events in the final selection after the single veto, the statistical error is also given. All Monte Carlo predictions are normalised to the integrated luminosity of the data.

detector and are easily rejected by the double veto. After the single veto, all background levels are almost negligible. Besides the requirement on the longitudinal momentum, most of the efficiency loss comes from the single veto, since the double veto rejects only events with two converted photons.

6 Experimental systematic errors

The efficiency of the selection is studied with a signal Monte Carlo simulation [24] including full detector simulation. It is found to be independent of the centre-of-mass energy and therefore the average efficiency is used to correct the data. The efficiency is about 97.8% in the barrel region and drops to 69% at the edge of the selection at $\cos\theta^* = 0.93$ as can be seen in Table 6. The total efficiency within $\cos\theta^* < 0.93$ is 92.6%. Uncertainties in the simulation give rise to the systematic errors as discussed below. The errors are given in % relative to the efficiency.

6.1 Cut values

To assess the stability of the cuts, the cut values are varied and the difference between data and Monte Carlo expectation is assigned as a systematic error. The kinematic cuts on energy sum, missing transverse and longitudinal momenta are changed by $\pm 10\%$. The cuts on the numbers of hits allowed in the neutral event selection are varied by one or two hits. The resulting systematic errors are at most 0.1% and in total contribute 0.17%.

6.2 Conversion probability

A crucial point for this analysis is the correct modelling of the material in the detector since this material leads to photon conversions. If a photon converts before the first active detector layer, a reliable distinction between a primary produced electron and a photon conversion is not possible. Events with such photons must be rejected from the analysis. Events with photons which convert later are selected and do not influence the efficiency.

The probabilities given in this paragraph are conversion probabilities for single photons and the given errors are absolute numbers. For $|\cos\theta| < 0.89$ the Monte Carlo prediction for the probability for a single photon to convert before SI is 0.7%. A systematic error of 0.2% is assigned to this value since the only material in front of the SI detector is the beam pipe which is uniform and therefore well modelled. There is, however, more material in the endcap e.g. from SI and CV readout electronics. In the region $0.89 < |\cos\theta| < 0.93$ the Monte Carlo prediction for the conversion probability in front of CV is 6 – 9%. Studies, for example, of the width of the ECAL energy distribution in Bhabha events show no significant disagreement in the Monte Carlo description of material in this region, and a 1% error is assigned to the conversion probability. For $|\cos\theta| > 0.93$ significant effects due to unmodelled material are clearly visible in these studies and this is the main reason for restricting the two highest-energy photons to

$|\cos\theta| < 0.93$. A 3% systematic error is assigned for additional photons with $|\cos\theta| > 0.93$. The Monte Carlo prediction for the conversion probability in this region is 10 – 15%.

Most events have two back-to-back photons. These photons hit equivalent kinds of material in the left and right side of the detector and consequently their conversion probabilities are correlated. For a two-photon event this leads to a systematic error on the efficiency of 0.4% in the region $|\cos\theta| < 0.89$. For a typical mixture of events at all angles the average systematic error on the efficiency is between 0.45% and 2.01%, where the 0.45% is taken to be correlated between $\cos\theta^*$ bins.

6.3 Angular reconstruction

Another important source of uncertainty is the reconstruction of the photon angle. A systematic mis-reconstruction of the angle would lead to distortions in the measured angular distribution. Monte Carlo studies show that the angular resolution is approximately $0.2^\circ - 0.3^\circ$, which makes a full unfolding unnecessary. However, some systematic shifts of up to 0.15° are predicted leading to a bias of the measured angular distribution. The Monte Carlo prediction of this bias is corrected via the efficiency bin-by-bin and is included in the efficiency given in Table 6. Since the angular reconstruction for photons cannot be cross-checked with the data the full size of the predicted bias is taken as a systematic error on the efficiency. For most of the central region this error is negligible, at other angles the error is between 2% and 3%. For the calculation of the total cross-section, these effects are only relevant at the edge of the phase-space of the selection, leading to an error of 0.46% corresponding to a shift of 0.15° at $\cos\theta^* = 0.93$.

While the event angle is mostly affected by shifts that are symmetric on both sides of the detector, the acollinearity is changed by shifts that are different on the left and right side. The error arising from such shifts is 0.1°.

6.4 Background

The expected background is very small. The Monte Carlo expectation for Standard Model processes, summarised in Table 4, is less than 4 events. Selected events in which one photon has hits in CV are scanned and the Standard Model background is estimated to be less than 10 events. Background from cosmic-ray events is estimated to be also less than 10 events by scanning selected events with at least one track segment in the muon chambers. For both these sources half of this estimate is corrected while the other half is taken as a systematic error. Since the angular distribution of the background is poorly known, to simplify the correction procedure, the shape of the signal distribution is assumed. Thus the background is corrected by increasing the efficiency by 0.2% corresponding to 10 events. A systematic error of 0.1% for each of the two sources is assigned.

6.5 Other errors

The efficiency loss due to overlaid cosmic-ray events[3] and noise hits in the detector is studied with randomly triggered beam crossings. This leads to expected signal rejection rates of 0.22% due to cosmic-ray events and 0.30% due to noise, corresponding to 12 and 16 events respectively. These numbers are cross-checked by scanning events and good agreement is found. The resulting efficiency loss of 0.52% is corrected for and a systematic error of 0.05% is assigned for each source.

The error due to Monte Carlo statistics enters only in the determination of the efficiency which leads to a very small binomial error of 0.1%. The radiative corrections are determined from $3 \cdot 10^9$ events, making the statistical error much smaller than the theoretical uncertainty and it is therefore neglected.

The luminosity errors are given in Table 1. The errors change slightly from energy to energy and are dominated by the systematic error. A total common error of 0.23% is assigned in order to simplify the error treatment in the log likelihood fits.

The trigger efficiency of the ECAL is tested with Bhabha events and is found to be 100%. The corresponding error is negligible.

6.6 Summary

In general the experimental systematic errors for this analysis are small. The largest errors arise from the conversion probability, the angular reconstruction and the luminosity. The overall systematic error for the total cross-section is 0.77%. For the differential cross-section the systematic error as a function of $\cos\theta^*$ is given in Table 6. For most of the central region the total systematic error is 0.56%, which is composed of 0.45% from the conversion probability, 0.23% from the luminosity, 0.17% from the cut values and small errors from the background and the efficiency loss. All systematic errors are independent of the centre-of-mass energy and fully correlated between energies.

7 Results

7.1 Cross-sections

The number of observed events in each class is given in Table 5 and compared to the number of events expected from Monte Carlo simulation. There is a good agreement for collinear events (class I), but there are fewer acollinear events observed than expected. To judge whether this is an indication for physics beyond the Standard Model one has to take into consideration that the main Monte Carlo generator includes only $\mathcal{O}(\alpha^3)$ terms. There is no Monte Carlo program available to calculate events with four photons in which one travels along the beam direction,

[3] A cosmic-ray particle in the detector which coincides with a signal event.

class	*I*	*II*	*III*	*IV*	
N_γ	≥ 2	2	3	3	≥ 4
observed	4747	394	71	20	3
expected	4730	435	94	–	5.3

Table 5: The number of observed and expected events in the different classes. The Monte Carlo prediction for classes *I* – *III* is from RADCOR. The expectation for class *IV* with four photons is calculated using FGAM. There is no Monte Carlo program available to generate events with three observed photons plus one escaping along the beam direction, hence no prediction for class *IV* events with three observed photons is given.

so no expectation is given for class *IV* events with three observed photons. Events with four observed photons are calculated using FGAM [25].

The most important discriminant for the classes is the acollinearity, the distribution of which is shown in Figure 3. The typical resolution is 0.35°. Discrepancies between data and Monte Carlo simulation at $\xi_{\rm acol} < 1^\circ$ may occur for two reasons. One is that Monte Carlo events with a soft third photon below some energy cut-off are generated with two exactly back-to-back photons. This affects the acollinearity distribution at $\xi_{\rm acol} < 1^\circ$ as can be seen in Figure 3. The other reason is the possible systematic shift of the reconstructed angle of about 0.1°. For larger values of $\xi_{\rm acol}$ differences are most likely due to missing higher order effects. The largest significance of a discrepancy between data and Monte Carlo simulation occurs for a cut of $\xi_{\rm acol} > 3^\circ$. In this case 1141 events are predicted with 1004 observed. Including a systematic error of 16 events due to the mismodelling of the angle, an excess in the Monte Carlo prediction of 3.6 standard deviations is observed. This discrepancy may be due to higher order effects, which can be large.

The measured differential cross-sections are plotted in Figure 4 for six energy ranges. Information for all eight energies can be found in Table 6. Integrating these distributions leads to the total cross-sections which are shown as a function of $\sqrt{s}$ in Figure 5 and are summarised in Table 7. The cross-sections are in very good agreement with the QED expectation. On average $\sigma_{\rm obs}/\sigma_{\rm QED} = 0.999 \pm 0.014 \pm 0.008$, where the first error is statistical and the second is systematic. This average has a $\chi^2/{\rm dof} = 12.7/7$ and includes the correlation of systematic errors. There is an additional error from theory of 0.01.

7.2 Tests of alternative models

Binned log likelihood fits for the alternative models are performed on the measured differential cross-sections taking systematic errors and their correlations into account. Where possible, the fit parameters, given in Table 8, are chosen such that the resulting probability distribution is approximately Gaussian. One-sided 95% confidence level limits are obtained for the fit parameters by renormalising the likelihood function to the physically allowed region in the same way as in [3]. The quoted limits on the model parameters correspond to these limits on the fit parameters. For excited electrons two types of fits are performed. Limits are determined on the coupling constant f_γ/Λ of an excited electron to an electron and a photon for various

$E_{\rm nom}$	183	189	192	196	200	202	205	207	efficiency		rad.cor.
$\cos\theta^*$-bin	events								ϵ	σ_ϵ/ϵ	$\mathcal{R}$
0.00−0.05	8	33	3	10	15	8	17	23	0.9515	0.0250	1.0689
0.05−0.10	21	37	5	18	10	6	14	20	0.9769	0.0056	1.0666
0.10−0.15	15	34	4	14	15	4	13	15	0.9769	0.0056	1.0644
0.15−0.20	10	40	7	15	12	3	11	22	0.9769	0.0056	1.0621
0.20−0.25	13	40	2	9	13	5	14	23	0.9769	0.0056	1.0599
0.25−0.30	14	43	10	11	13	2	8	27	0.9769	0.0056	1.0577
0.30−0.35	20	47	10	14	20	7	29	26	0.9755	0.0056	1.0556
0.35−0.40	22	41	15	22	21	17	12	23	0.9753	0.0056	1.0534
0.40−0.45	21	38	12	19	11	9	18	18	0.9753	0.0056	1.0512
0.45−0.50	13	49	8	22	15	6	17	31	0.9753	0.0056	1.0492
0.50−0.55	21	61	7	23	24	10	22	23	0.9742	0.0056	1.0471
0.55−0.60	23	72	6	25	25	18	21	37	0.9742	0.0056	1.0451
0.60−0.65	25	64	14	38	24	19	21	48	0.9742	0.0056	1.0433
0.65−0.70	24	96	18	35	33	17	37	68	0.9762	0.0056	1.0415
0.70−0.75	36	104	18	42	34	23	50	75	0.9906	0.0208	1.0399
0.75−0.80	48	131	23	59	53	19	47	81	0.9824	0.0208	1.0387
0.80−0.85	66	176	33	71	72	35	71	89	0.9647	0.0208	1.0380
0.85−0.90	78	255	32	102	75	48	84	145	0.8976	0.0220	1.0387
0.90−0.93	60	170	31	67	69	25	60	97	0.6937	0.0286	1.0412

Table 6: Measured angular distributions. For each centre-of-mass energy and $\cos\theta^*$ bin the number of observed events is given. The last columns give the efficiency, its relative systematic error and the radiative correction which has an error of 0.01. The efficiency includes the corrections due to the background and the rejection because of noise and overlaid cosmic-ray events. For the systematic error on the efficiency the common contribution of 0.56% is taken as correlated between bins.

$\sqrt{s}$	Born cross-section [pb]	
[GeV]	observed	QED
182.68	10.05±0.43±0.08	9.32
188.63	8.79±0.23±0.07	8.74
191.59	9.24±0.58±0.07	8.47
195.53	8.43±0.34±0.07	8.13
199.52	7.39±0.31±0.06	7.81
201.63	7.88±0.47±0.06	7.65
204.88	7.40±0.31±0.06	7.42
206.56	6.78±0.23±0.05	7.29

Table 7: The measured and predicted total cross-sections at Born level within the angular range of $\cos\theta^* < 0.93$. The measured values are shown with their statistical and systematic errors. The additional uncertainty on the theoretical prediction is about 1%.

masses M_{e^*}. The resulting limits shown in Figure 6 do not depend on a special choice of Λ. A limit on the mass M_{e^*} for a fixed coupling constant $f_\gamma = 1$ is also determined. In this case the scale Λ is fixed to M_{e^*} and no fit parameter can be found to give a Gaussian probability distribution. Therefore the likelihood distribution is shown in Figure 7. To make the Standard Model value at $M_{e^*} = \infty$ visible the likelihood is plotted as a function of $M_{e^*}^{-4}$. The limit of $M_{e^*} > 245$ GeV is obtained at $\Delta\text{LogL} \equiv -\ln\mathcal{L} + \ln\mathcal{L}_{\max} = 1.92$.

All fit results are summarised in Table 8. The limits on the model parameters are stronger by 10% to 20% than our previously published limits [3]. Limits on the excited electron coupling f_γ/Λ are much weaker than the limits obtained from direct searches [40] but extend beyond the kinematic limit for excited electron production as can be seen in Figure 8. As a comparison limits from excited electron production via electron-γ fusion determined by H1 [41] are also shown. Similar results are available from ZEUS [42].

Fit parameter	Fit result	95% CL Limit [GeV]
$\Lambda_\pm^{-4}$	$\left(-40.3^{+37.2}_{-36.5}\right)$ TeV^{-4}	$\Lambda_+ > 371$ $\Lambda_- > 314$
Λ'^{-6}	$\left(-3.56^{+2.84}_{-2.77}\right)$ TeV^{-6}	$\Lambda' > 800$
λ/M_s^4	$\left(0.926^{+0.850}_{-0.858}\right)$ TeV^{-4}	$\lambda = +1$: $M_s > 805$ $\lambda = -1$: $M_s > 956$
$M_{e^*}(f_\gamma = 1;\ \Lambda = M_{e^*})$	see Figure 7	$M_{e^*} > 245$
$(f_\gamma/\Lambda)^4(M_{e^*} = 200$ GeV$)$	$\left(-215^{+201}_{-196}\right)$ TeV^{-4}	$f_\gamma/\Lambda < 4.11$ TeV^{-1}

Table 8: Fit results and limits at 95% confidence level obtained from binned log likelihood fits to the differential cross-sections. The model parameters are defined in Section 4.

7.3 Resonance production

Of the 71 selected class *III* events, 64 have all three photons within $|\cos\theta| < 0.93$. These events are used to search for a photonically decaying resonance X which is produced in association with a photon ($e^+e^- \to \gamma X\ ,\ X \to \gamma\gamma$). Each event is a candidate for three different masses corresponding to the pairing of the photons. For planar three photon events three-body kinematics can be used to calculate the energies E_k of the photons:

$$E_k \propto \sin\alpha_{ij}\ ;\ E_1 + E_2 + E_3 = \sqrt{s}\ , \tag{11}$$

where E_k is the energy of one photon and α_{ij} is the angle between the other two photons. This leads to a resolution on the invariant mass of photon pairs of about 0.5 GeV. Calculating the mass from the observed cluster energies would result instead in a resolution of about 3%.

For the signal it is assumed that the resonance X has isotropic production and decay distributions. The QED background on the other hand is peaked in the forward direction. Since the

$\sqrt{s}$ [GeV]	Mass [GeV]			$\sqrt{s}$ [GeV]	Mass [GeV]		
181.73	51.7	84.1	152.6	195.47	100.3	108.4	128.1
182.41	47.7	83.5	155.0	199.55	56.2	126.9	143.3
182.72	55.7	73.8	157.6	199.56	43.1	114.3	157.8
182.75	58.7	49.5	165.8	199.57	81.3	48.3	175.7
182.75	42.7	68.4	164.0	195.59	56.0	106.5	154.2
182.86	60.1	118.2	125.9	195.59	80.3	82.9	158.0
182.89	89.0	104.2	121.1	199.41	90.0	96.8	149.3
182.70	51.3	103.2	141.8	199.45	78.3	121.1	137.8
182.70	67.6	116.3	123.6	199.52	99.3	116.3	128.1
182.70	69.5	84.1	146.5	201.58	40.8	127.3	150.9
188.58	60.4	50.7	171.3	201.63	81.8	118.9	140.8
188.59	43.5	88.8	160.6	202.55	49.3	99.4	169.5
188.59	79.9	69.0	156.2	203.66	83.1	78.0	168.8
188.59	102.2	78.8	137.5	204.65	26.2	127.3	158.1
188.60	33.6	94.8	159.5	204.73	51.4	86.8	178.2
188.61	76.3	102.7	138.5	205.04	54.9	64.9	186.6
188.62	49.5	73.7	166.4	205.11	60.5	78.2	179.7
188.63	66.5	45.9	170.4	205.13	65.0	84.6	175.2
188.63	51.1	76.0	164.9	205.14	62.5	93.9	171.4
188.64	105.7	97.8	121.8	205.35	37.7	137.0	148.3
188.65	37.9	98.7	156.3	205.81	73.1	120.4	150.0
188.66	115.3	99.0	111.8	206.03	62.4	84.4	177.3
188.66	35.7	94.4	159.4	206.17	63.1	64.2	185.5
188.66	67.6	65.8	163.4	206.17	58.4	103.1	168.7
188.67	93.0	77.9	144.5	206.39	54.2	92.4	176.4
188.67	35.1	96.4	158.3	206.55	66.0	116.7	157.2
188.67	54.7	86.3	158.6	206.56	93.8	104.1	151.8
188.67	65.4	92.8	150.7	206.57	83.3	65.0	177.5
189.01	34.4	99.3	157.1	206.58	105.5	125.5	125.7
191.52	41.2	84.4	166.9	206.61	69.6	108.7	161.4
191.63	43.2	116.9	145.6	207.96	69.9	84.9	176.5
195.47	61.5	83.3	165.8	208.03	43.1	112.1	169.9

Table 9: The three invariant masses for planar three photon events. The events are grouped according to the energy ranges given in Table 1.

QED Monte Carlo generator appears to overestimate the production of three-photon events the background is scaled to the number of observed events.

The efficiency for resonance production can be separated into two parts. The first part accounts for the restricted phase-space of the selection summarised in Equation 12:

$$|\cos\theta_i| < 0.93,\ i = 1,2,3\ ;\ \xi_{\rm acol} > 10^\circ\ . \tag{12}$$

This efficiency depends strongly on the mass, $M_{\rm X}$, of the resonance. At a centre-of-mass energy of 207 GeV it is between 64% and 72% for masses in the range 70 GeV to 170 GeV. The mass range is limited by the acollinearity cut. The second part is the reconstruction efficiency for Xγ events within the phase-space defined by Equation 12; this depends only weakly on $M_{\rm X}$ and the centre-of-mass energy. It is 96.3% which is larger than the efficiency for QED events because of the different angular distribution.

The observed distribution of the invariant mass of photon pairs is shown in Figure 9 together with the distribution expected for a signal at $M_{\rm X} = 131.5$ GeV. A list of the three invariant masses per event can be found in Table 9. Limits at 95% confidence level on the product of Xγ production cross-section and branching ratio are derived using a method of fractional event counting [43], where the weight of an event is determined according to the resolution and the difference between hypothetical and reconstructed masses. The intrinsic width of the resonance X is assumed to be negligible. The limits are calculated assuming that the cross-section is independent of $\sqrt{s}$. If the production cross-section depends on $\sqrt{s}$, the limit can be used with respect to the luminosity weighted centre-of mass energy of $\langle\sqrt{s}\rangle$ =196.6 GeV. For most production cross-sections (e.g. $\sigma \propto 1/s$ or $\propto \ln s$) the difference from the correctly scaled limit is less than 0.8% for masses in the range 40 GeV to 170 GeV. For a threshold behaviour like $\sigma \propto (1 - \frac{M_{\rm X}^2}{s})^3$ [18] this holds only up to $M_{\rm X} < 145$ GeV. The limits are about a factor two better than our previously published results [3].

8 Conclusion

Total and differential cross-sections for the process $\mathrm{e^+e^-} \to \gamma\gamma(\gamma)$ have been measured at high energies with a large data set. The data are in good agreement with the QED expectation, though some discrepancies in the acollinearity distribution are observed, which are attributed to missing higher order effects in the $\mathcal{O}(\alpha^3)$ model calculations. Strong constraints on models predicting deviations from QED are obtained which are summarised in Table 8. Lower limits at 95% confidence level are placed on cut-off parameters $\Lambda_\pm$ of about 340 GeV and on the scale of gravity in extra dimensions of about 880 GeV. Excited electrons must be heavier than 245 GeV if the relative strength of the $\mathrm{e^*e}\gamma$ vertex is $f_\gamma/\Lambda = 1/M_{\mathrm{e^*}}$. Limits on this coupling are placed for a range of excited electron masses. In the mass spectrum of photon pairs no indication for a narrow resonance X is found leading to limits on cross-section times branching ratio for Xγ production with $\mathrm{X} \to \gamma\gamma$ of about 0.02 pb assuming isotropic production and decay distributions.

Acknowledgements:

We particularly wish to thank the SL Division for the efficient operation of the LEP accelerator at all energies and for their close cooperation with our experimental group. In addition to the support staff at our own institutions we are pleased to acknowledge the
Department of Energy, USA,
National Science Foundation, USA,
Particle Physics and Astronomy Research Council, UK,
Natural Sciences and Engineering Research Council, Canada,
Israel Science Foundation, administered by the Israel Academy of Science and Humanities,
Benoziyo Center for High Energy Physics,
Japanese Ministry of Education, Culture, Sports, Science and Technology (MEXT) and a grant under the MEXT International Science Research Program,
Japanese Society for the Promotion of Science (JSPS),
German Israeli Bi-national Science Foundation (GIF),
Bundesministerium für Bildung und Forschung, Germany,
National Research Council of Canada,
Hungarian Foundation for Scientific Research, OTKA T-029328, and T-038240,
Fund for Scientific Research, Flanders, F.W.O.-Vlaanderen, Belgium.

References

[1] OPAL Collaboration, K. Ackerstaff *et al.*, Eur. Phys. J. **C1** (1998) 21.

[2] OPAL Collaboration, K. Ackerstaff *et al.*, Phys. Lett. **B438** (1998) 379.

[3] OPAL Collaboration, G. Abbiendi *et al.*, Phys. Lett. **B465** (1999) 303.

[4] ALEPH Collaboration, A. Heister *et al.*, submitted to Eur. Phys. J. (2002), CERN-EP-2002-033.

[5] ALEPH Collaboration, R. Barate *et al.*, Phys. Lett. **B429** (1998) 201.

[6] DELPHI Collaboration, P. Abreu *et al.*, Phys. Lett. **B433** (1998) 429.

[7] DELPHI Collaboration, P. Abreu *et al.*, Phys. Lett. **B491** (2000) 67.

[8] L3 Collaboration, P. Achard *et al.*, Phys. Lett. **B531** (2002) 28.

[9] L3 Collaboration, M. Acciarri *et al.*, Phys. Lett. **B475** (2000) 198.

[10] L3 Collaboration, M. Acciarri *et al.*, Phys. Lett. **B413** (1997) 159.

[11] L3 Collaboration, M. Acciarri *et al.*, Phys. Lett. **B384** (1996) 323.

[12] S. D. Drell, Ann. Phys. **4** (1958) 75.

[13] O. J. P. Eboli, A. A. Natale, and S. F. Novaes, Phys. Lett. **B271** (1991) 274.

[14] F. E. Low, Phys. Rev. Lett. **14** (1965) 238.

[15] P. Mery, M. Perrottet, and F. M. Renard, Z. Phys. **C38** (1988) 579.

[16] K. Agashe and N. G. Deshpande, Phys. Lett. **B456** (1999) 60.

[17] O. J. P. Eboli *et al.*, Phys. Lett. **B434** (1998) 340.

[18] R. Brustein and D. H. Oaknin, Phys. Rev. **D62** (2000) 015001.

[19] OPAL Collaboration, P. D. Acton *et al.*, Phys. Lett. **B311** (1993) 391.

[20] DELPHI Collaboration, P. Abreu *et al.*, Phys. Lett. **B458** (1999) 431.

[21] OPAL Collaboration, K. Ahmet *et al.*, Nucl. Instrum. Meth. **A305** (1991) 275.

[22] OPAL Collaboration, S. Anderson *et al.*, Nucl. Instrum. Meth. **A403** (1998) 326.

[23] OPAL Collaboration, B. E. Anderson *et al.*, IEEE Trans. Nucl. Sci. **41** (1994) 845.

[24] F. A. Berends and R. Kleiss, Nucl. Phys. **B186** (1981) 22.

[25] CALKUL Collaboration, F. A. Berends *et al.*, Nucl. Phys. **B239** (1984) 395.

[26] S. Jadach, W. Placzek, and B. F. L. Ward, Phys. Lett. **B390** (1997) 298.

[27] D. Karlen, Nucl. Phys. **B289** (1987) 23.

[28] S. Jadach, B. F. L. Ward, and Z. Was, Comput. Phys. Commun. **66** (1991) 276.

[29] G. Montagna *et al.*, Nucl. Phys. **B541** (1999) 31.

[30] T. Sjostrand, Comput. Phys. Commun. **39** (1986) 347.

[31] T. Sjostrand and M. Bengtsson, Comput. Phys. Commun. **43** (1987) 367.

[32] OPAL Collaboration, J. Allison *et al.*, Nucl. Instrum. Meth. **A317** (1992) 47.

[33] W. Heitler, Quantum Theory of Radiation, (Oxford University Press, second edition, 1944), pages 204–207.

[34] M. Capdequi Peyranere, Y. Loubatieres, and M. Talon, Nucl. Phys. **B249** (1985) 61.

[35] J. Fujimoto, M. Igarashi, and Y. Shimizu, Prog. Theor. Phys. **77** (1987) 118.

[36] S. J. Brodsky and S. D. Drell, Phys. Rev. **D22** (1980) 2236.

[37] F. M. Renard, Phys. Lett. **B116** (1982) 264.

[38] B. Vachon, *Excited electron contribution to the* $e^+e^- \to \gamma\gamma$ *cross-section*, hep-ph/0103132, 2001.

[39] I. Antoniadis *et al.*, Phys. Lett. **B436** (1998) 257.

[40] OPAL Collaboration, G. Abbiendi *et al.*, submitted to Phys. Lett. (2002), hep-ex/0206061.

[41] H1 Collaboration, C. Adloff *et al.*, Eur. Phys. J. **C17** (2000) 567.

[42] ZEUS Collaboration, S. Chekanov *et al.*, submitted to Phys. Lett. (2001), hep-ex/0109018.

[43] P. Bock, *Determination of exclusion limits for particle production using different decay channels with different energies, mass resolutions and backgrounds*, Heidelberg preprint HD-PY 96/05, 1996.

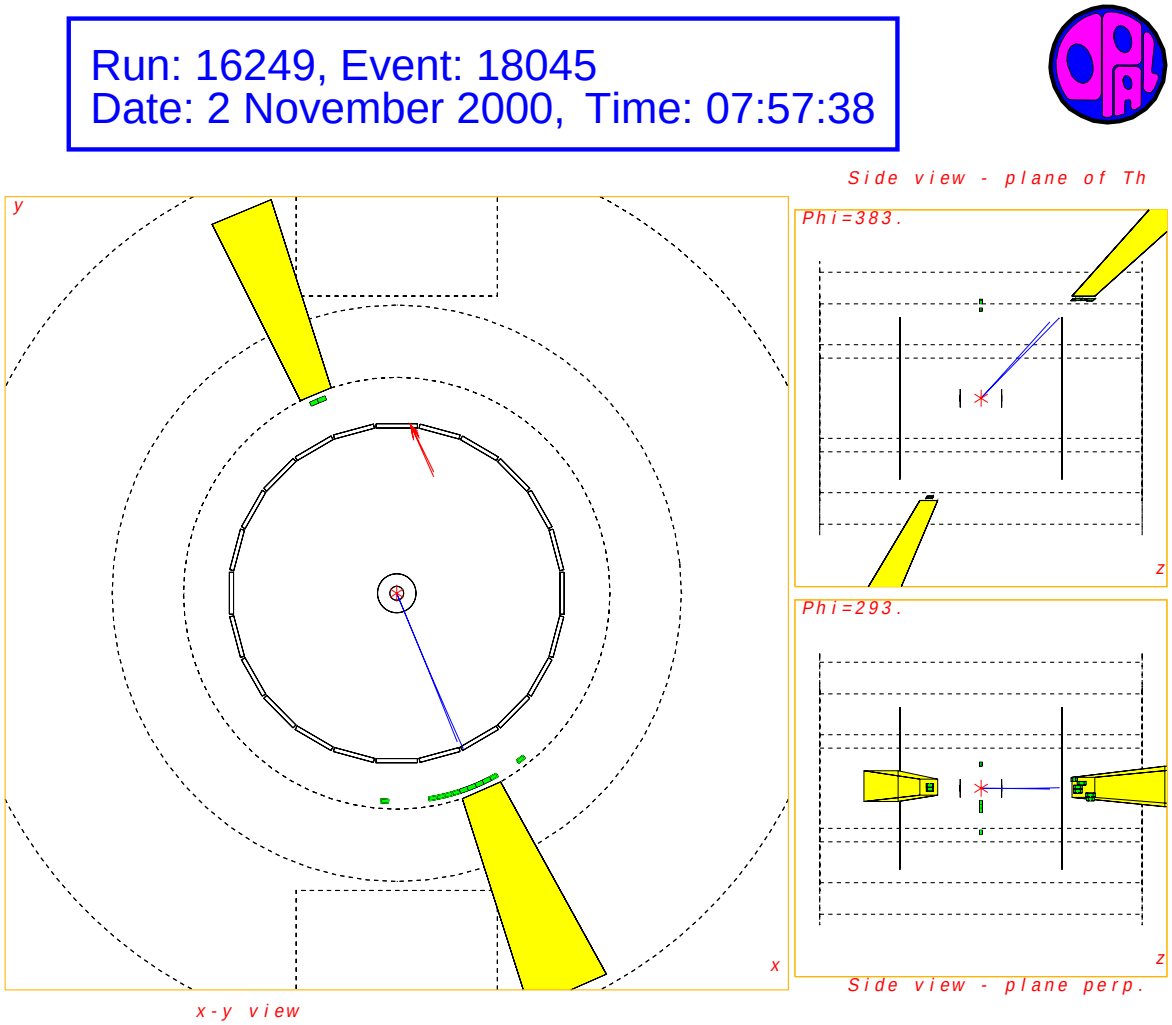

Figure 1: Last OPAL $e^+e^- \to \gamma\gamma(\gamma)$ event, taken three minutes before the final shut-down of LEP. Two high-energy clusters are detected in the electromagnetic calorimeter. This is a class *II* event with acollinearity $\xi_{\rm acol} = 17°$. One photon has converted between CV and CJ; the two corresponding tracks are visible in the tracking chambers.

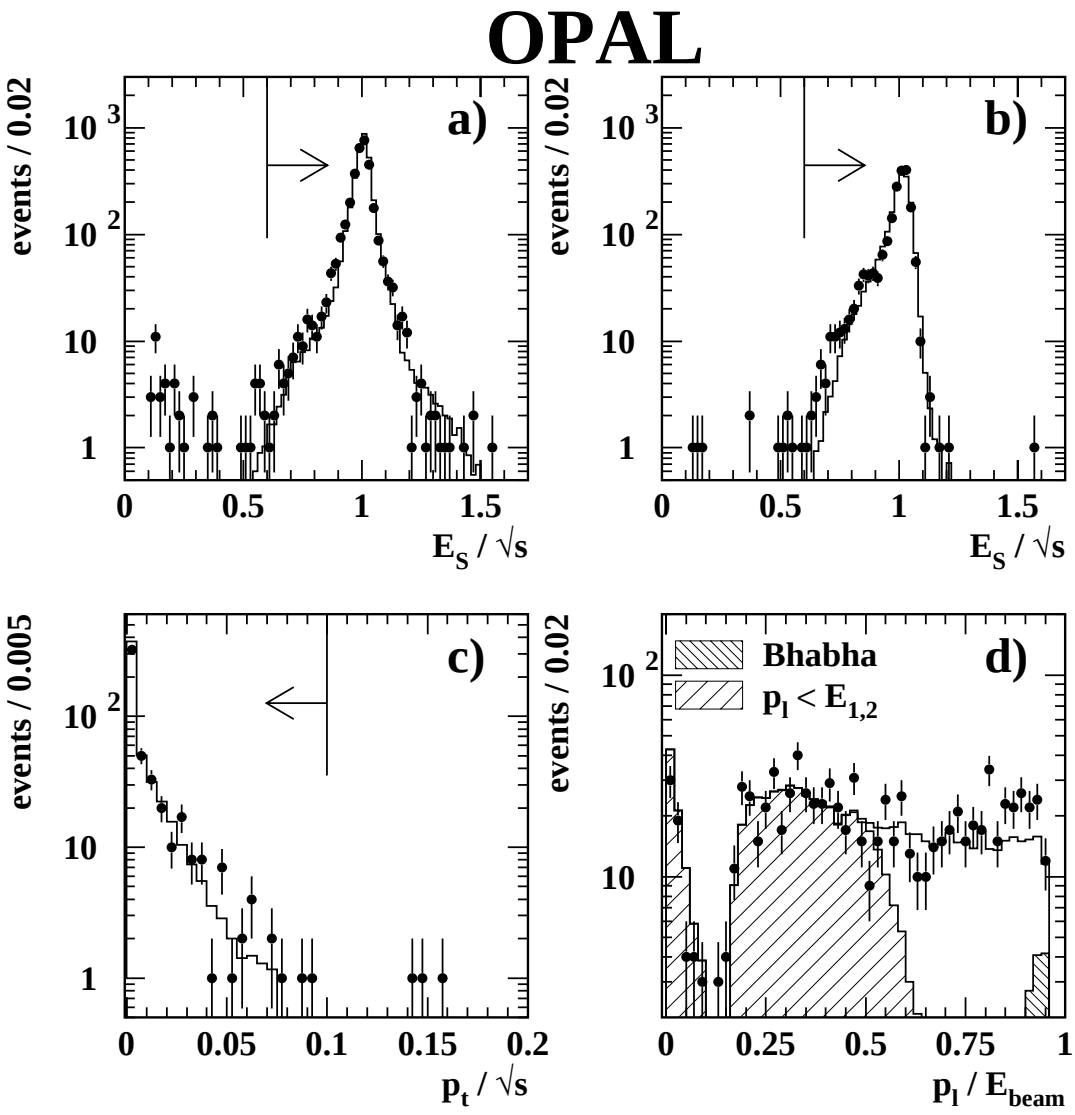

Figure 2: Distributions used in the kinematic event selection. The energy sum for events of all classes is shown for barrel and endcap regions separately in plots a) $\cos\theta^* < 0.81$ and b) $\cos\theta^* \geq 0.81$. For events that are not in class I plot c) shows the transverse momentum and d) the longitudinal momentum. The points are the OPAL data after application of all cuts except that on the quantity which is plotted. The histograms show the Monte Carlo expectation. The arrows in a), b) and c) show the positions of the cuts. For the longitudinal momentum there is no cut at a specific value, events are selected if $p_1 < E_{1,2}$ as indicated by the Monte Carlo distribution shown as the shaded histogram. Background comes mainly from cosmic-ray events. In plot d) some Bhabha background is visible.

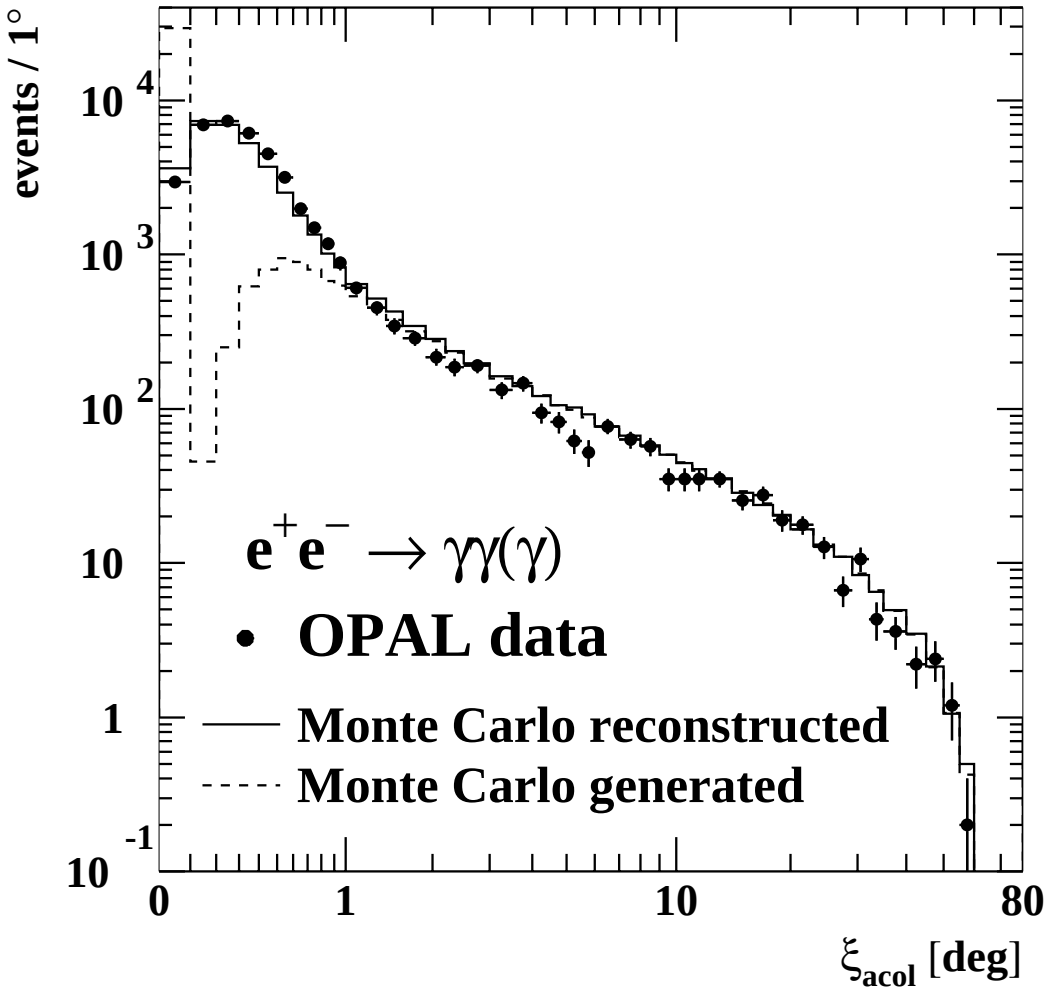

Figure 3: Acollinearity $\xi_{\rm acol}$ for all selected events. Because of the non-uniform bin size the entries are normalised to events/1°. The measured distribution is compared to the $\mathcal{O}(\alpha^3)$ Monte Carlo prediction including full detector simulation. The Monte Carlo distribution at generator level is also shown. The resolution is about 0.35° and the possible systematic bias on the angle is around 0.1°.

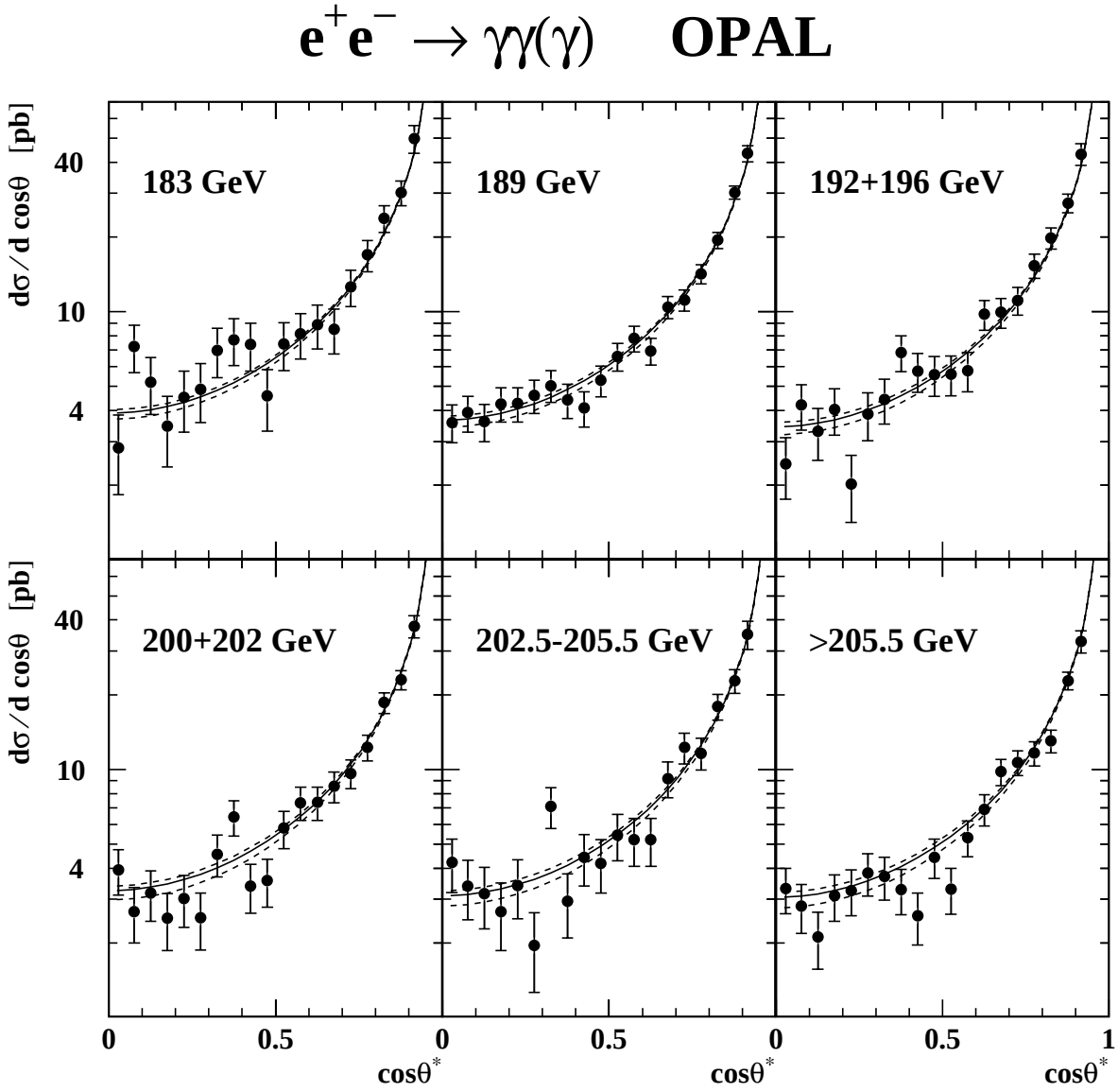

Figure 4: The measured differential cross-section at the Born level for the process $e^+e^- \to \gamma\gamma(\gamma)$ for six ranges of centre-of-mass energy. The points show the number of observed events corrected for efficiency and radiative effects. The solid curve corresponds to the Born-level QED prediction. The dashed lines represent the 95% confidence level interval from the fit to the function given in Equation 3.

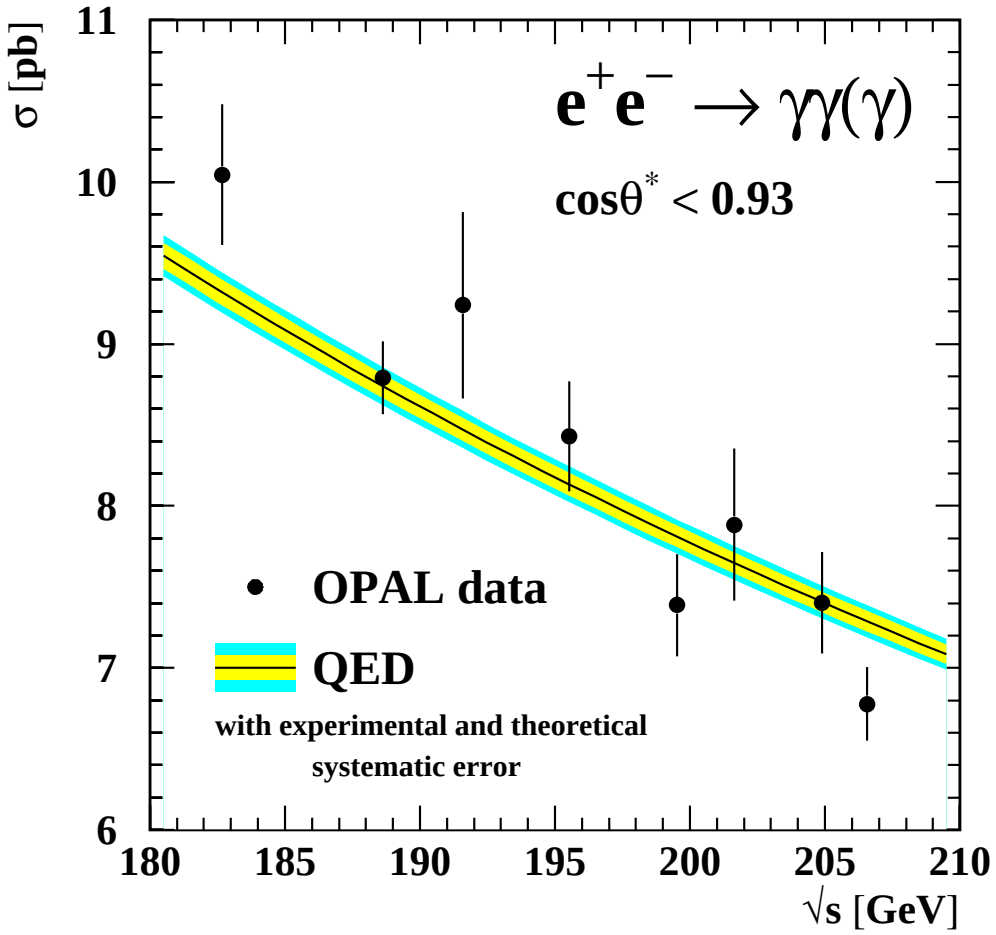

Figure 5: Total cross-section at the Born level for the process $e^+e^- \to \gamma\gamma(\gamma)$ with $\cos\theta^* < 0.93$. The curve corresponds to the Born-level QED expectation. The data are corrected for efficiency loss and higher-order effects. The errors shown for the measurements are statistical only. The systematic errors are correlated between energies and are plotted as a band around the QED expectation. The inner band represents the experimental error and the outer band includes the theoretical error.

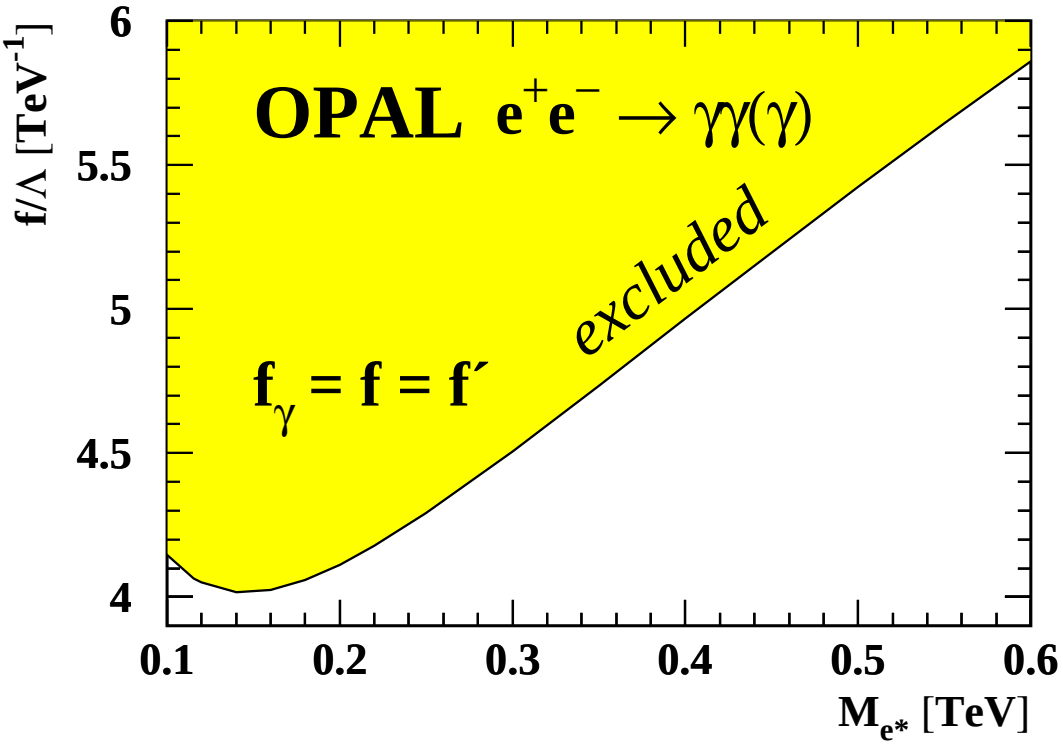

Figure 6: Upper limit at 95% confidence level on the coupling f_γ/Λ as a function of the mass M_{e^*} of an excited electron.

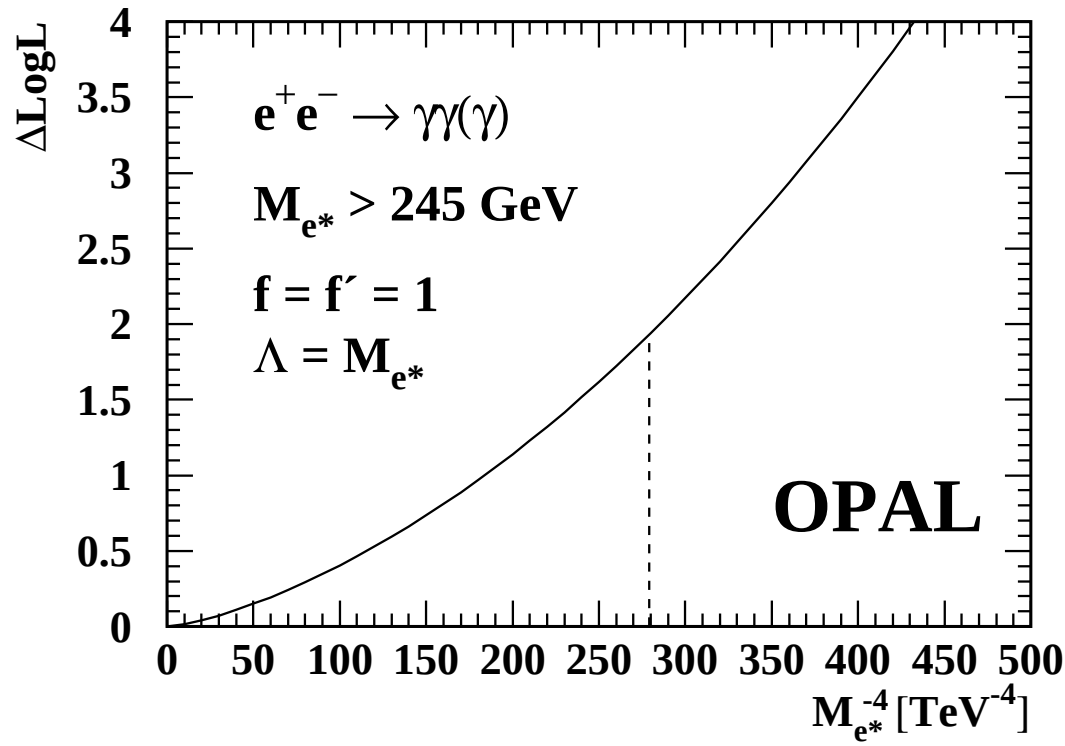

Figure 7: Likelihood difference as a function of $M_{e^*}^{-4}$ for fixed $f_\gamma = 1$ and $\Lambda = M_{e^*}$. The limit obtained at $\Delta\text{LogL} = 1.92$ is $M_{e^*} > 245$ GeV.

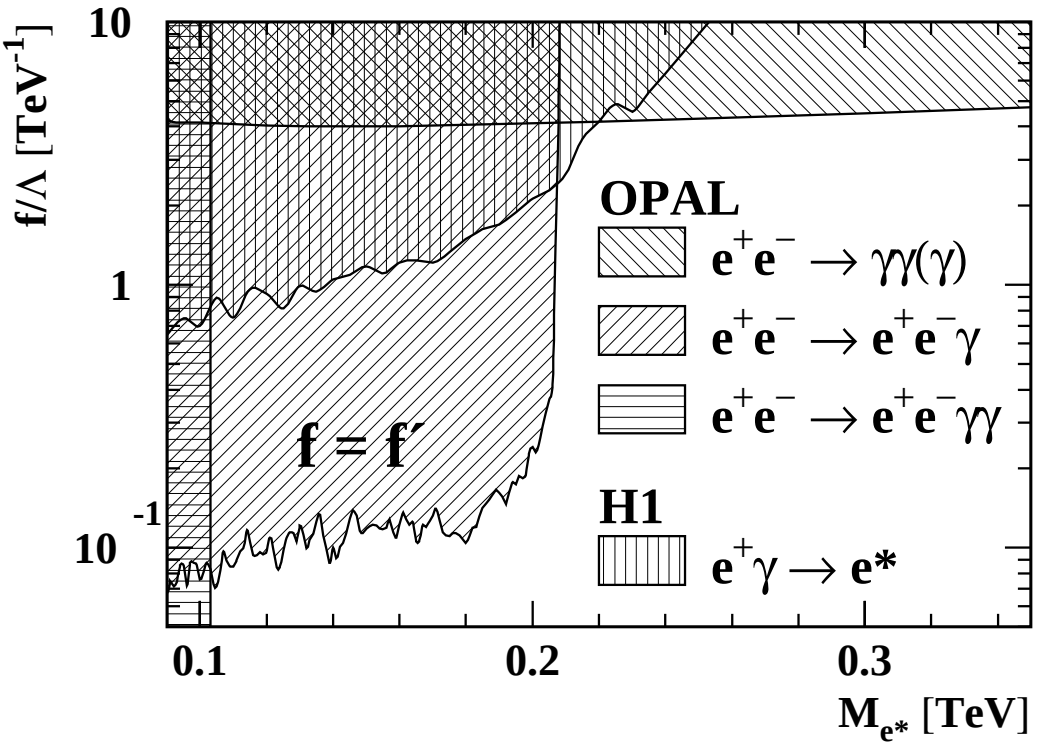

Figure 8: Comparison of limits on the coupling of excited electrons. OPAL results are given from this analysis and the two channels of the direct search [40] together with the results from H1 [41]. The shaded regions are excluded at 95% confidence level in each case.

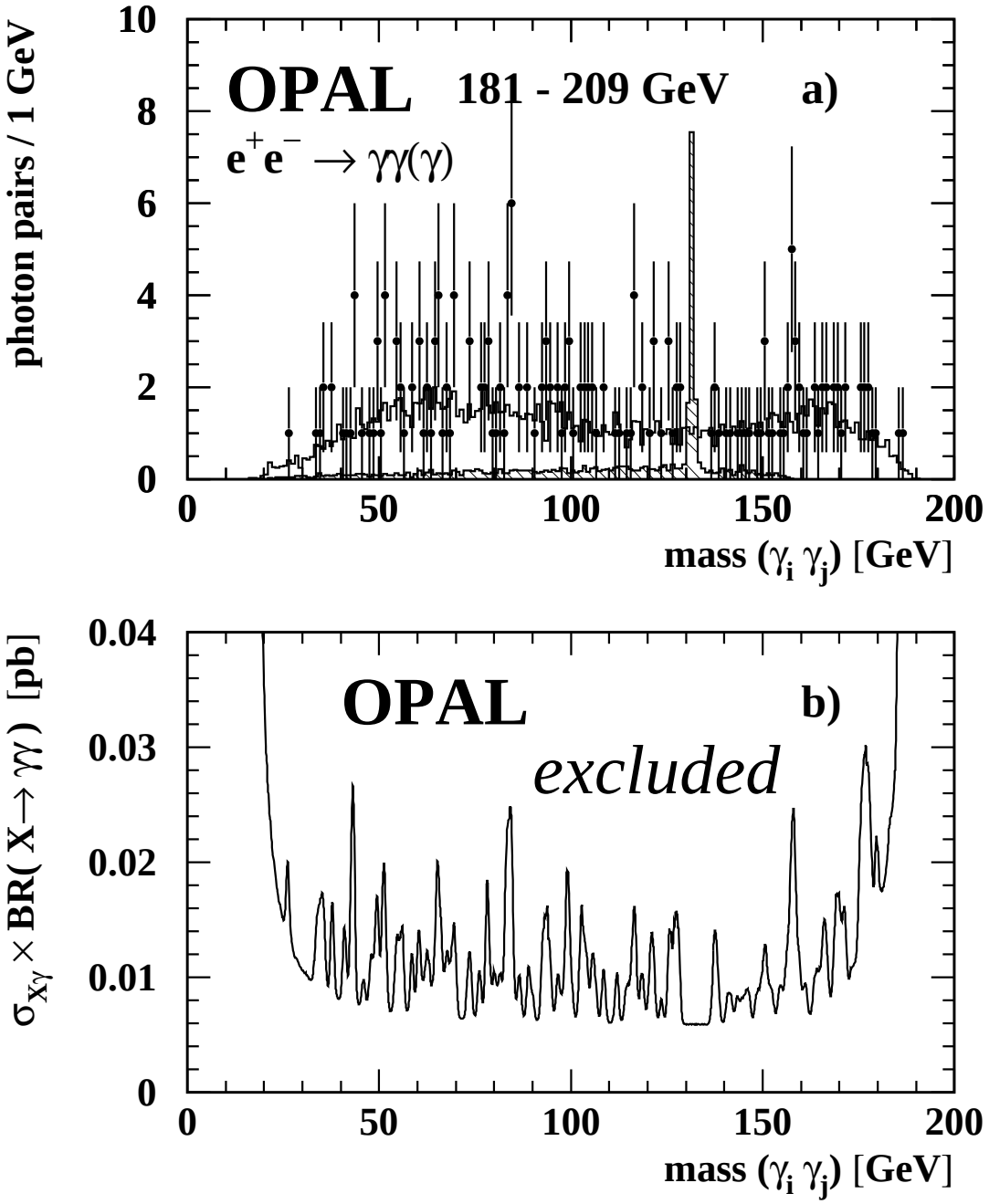

Figure 9: Results of a search for resonance production in class *III* events. a) shows the invariant mass of photon pairs for data (points) and for the $e^+e^- \to \gamma\gamma\gamma$ Monte Carlo expectation (histogram) scaled to the number of observed events. There are three photon pairs per event. A hypothetical signal with $\sigma_{X\gamma} \times BR = 0.02$ pb and a mass $M_X = 131.5$ GeV is superimposed (hatched histogram). The binning is chosen to match the expected mass resolution. b) shows the upper limit at 95% confidence level for the product of production cross-section and branching ratio for the process $e^+e^- \to X\gamma$, $X \to \gamma\gamma$ as a function of the mass of the resonance X.